ELSEVIER

International Journal of Heat and Fluid Flow 22 (2001) 424–432

International Journal of HEAT AND FLUID FLOW

www.elsevier.com/locate/ijhff

Thermal and fluid dynamic behavior of symmetrically heated vertical channels with auxiliary plate

Assunta Andreozzi, Oronzio Manca *

Dipartimento di Ingegneria Aerospaziale, Seconda Universitá degli Studi di Napoli, Real Casa dell'Annunziata via Roma 29, 81031 Aversa (CE), Italy

Received 15 February 2000; accepted 20 January 2001

Abstract

Air natural convection in vertical channel configurations is strongly attractive in thermal design and control of devices. This is mainly due to its simplicity, no maintenance costs and reliability. This paper examines air natural convection in vertical channels with an auxiliary plate along the centerline. The channel is symmetrically heated and the walls are at uniform heat flux, whereas the auxiliary plate is either adiabatic or heated at uniform heat flux. The analysis is obtained for a two-dimensional steady state and laminar regime, and the fully elliptic equations are solved numerically by the control volume method on a finite I-shaped computational domain. Results in terms of stream function and temperature fields, velocity and temperature profiles inside the channel and pressure profiles along the centerline are given either for insulated auxiliary plate or for heated auxiliary plate. The adiabatic auxiliary plate along the centerline of the channel produces a chimney effect reduction of the channel while the heated auxiliary plate, at higher Ra values (10^5–10^6), provides an increase in the mass flow rate in the channel. Finally, two correlations between average channel Nusselt number, channel Rayleigh number, Ra^*, and dimensionless auxiliary plate height, h/L, are proposed. One correlation is for the channel with heated auxiliary plate and another is for the channel with unheated auxiliary plate. The channel Rayleigh number range is 10^2–10^5 and the dimensionless auxiliary plate height, h/L, is in the range $[0, 1]$.

Keywords: Air natural convection; Chimney effect; Auxiliary plate; Numerical solution

1. Introduction

Engineering applications of natural convection in vertical heated channels are many and some examples are thermal control, solar collectors, nuclear reactors, etc. (Gebhart et al., 1988; Peterson and Ortega, 1990; Raithby and Hollands, 1998). Therefore natural convection in vertical channels has been extensively analyzed by means of numerical approach (Campo et al., 1999). The knowledge of thermal and fluid dynamic fields, such as temperature, velocity and pressure, provides basic guidelines in the design of devices in passive thermal control by means of natural convection.

Nowadays, the main purposes of natural convection analysis in channels are the thermal optimization of simple configurations (Morrone et al., 1997) and/or the thermal design of modified configurations derived from the simple channel, which could enhance heat transfer. This is well documented by Ledezma and Bejan (1997), Kim and Lee (1996) and Bar-Cohen and Kraus (1988).

In recent years almost all modified configurations of the simple channel have been studied numerically. Some of these configurations are the vertical channel with a modified inlet zone (Roberts and Floryan, 1998), with adiabatic extension upstream and downstream (Lee, 1994; Straatman et al., 1993; Oosthuizen, 1984; Campo et al., 1997, 1999) and with an auxiliary plate along the centerline of the channel (Aihara et al., 1996; Cheng et al., 1988; Naylor and Tarasuk, 1993; Floryan and Novak, 1994; Andreozzi et al., 1999).

The symmetrically heated channel at uniform heat flux with auxiliary plate has rarely been investigated with the exception of Andreozzi et al. (1999). In fact, the first author who introduced this configuration was Aihara in 1963, as reported in Aihara et al. (1996). He claimed that the shorter auxiliary plate heated at the same temperature as the channel walls increased the heat transfer compared to the simple channel. Recently, Naylor and Tarasuk studied the divided vertical channel numerically (1993a) and experimentally (1993b). In the numerical paper they employed both the elliptic and parabolic Navier–Stokes equations, which were solved by FIDAP program. The inlet channel conditions were based on the Jeffrey–Hamel flow. More recently, Floryan and Novak (1994) numerically investigated multiple parallel vertical channels, by employing the FIDAP program. An analogous configuration was previously investigated by Sparrow and Tao (1982). They analyzed two

* Corresponding author. Tel.: +39-08150102041203; fax: +39-0815010204.

E-mail address: manca@unina.it (O. Manca).

0142-727X/01/$ - see front matter
PII: S0142-727X(01)00080-7

Notation

a	thermal diffusivity, m^2/s
b	channel gap, m
g	gravity acceleration, m/s^2
Gr	Grashof number, Eq. (5)
h	auxiliary plate height, m
$h(x)$	local convective coefficient, W/m^2 K
k	thermal conductivity, W/m K
L	channel plate height, m
L_x	height of the reservoir, m
L_y	width of the reservoir, m
n_X	number of nodes along X
n_Y	number of nodes along Y
$Nu(x)$	local Nusselt number
Nu	average Nusselt number
p	pressure, Pa
P	dimensionless pressure, Eq. (5)
Pr	Prandtl number, Eq. (5)
$\dot{q}$	heat flux, W/m^2
Ra	Rayleigh number, Eq. (5)
Ra^*	channel Rayleigh number, Eq. (5)
T	temperature, K
u, v	velocity components along x, y, m/s
U, V	dimensionless velocities, Eq. (5)
x_q	heat flux ratio, Eq. (5)
x, y	Cartesian coordinates, m
X, Y	dimensionless coordinates

Greeks

β	volumetric coefficient of expansion, 1/K
Δ	difference between two values
θ	dimensionless temperature, Eq. (5)
ν	kinematic viscosity, m^2/s
ψ	stream function, m^2/s
Ψ	dimensionless stream function, Eq. (5)
ρ	density, kg/m^3
ω	vorticity, 1/s
Ω	dimensionless vorticity, Eq. (5)

Subscripts

∞	free stream condition
max	maximum value
w_1	channel wall
w_2	center line
p	auxiliary plate
c	channel
av	average value
0	refers to the channel without auxiliary plate ("base case")

vertical parallel channels that share a common wall across which heat is transferred from one channel to the other. The gap between the two channels was different. They solved numerically the parabolic set of equations with a finite difference scheme. Andreozzi et al. (1999) studied the configuration symmetrically heated with the walls at uniform heat flux and the auxiliary plate was either insulated or heated at uniform heat flux. The analysis was carried out by means of a finite volume method which solved the fully elliptic problem. The finite computational domain consisted of the channel and one reservoir upstream and another downstream.

The motivation of the present study is to further investigate the thermal and fluid dynamic behavior of the configuration studied in Andreozzi et al. (1999). In particular the stream function and temperature fields, the velocity and temperature profiles inside the channel and the pressure profiles along the centerline of the computational domain are provided. The results are obtained for air, Rayleigh number, Ra, equal to 10^3–10^6, channel aspect ratio L/b equal to 10 and dimensionless auxiliary plate height h/L ranges in $[0, 1]$. Finally, two correlations between average channel Nusselt number, channel Rayleigh number and a dimensionless geometric parameter, h/L, are proposed.

2. Mathematical and geometrical formulation

The studied configuration is made of two vertical parallel plates uniformly heated and a very thin auxiliary plate placed in the mid-plane of the two parallel plates. In Fig. 1(a) the investigated geometry is shown. The height of the plates is L, the distance between the two plates is b and the height of the auxiliary plate is h. The h value ranges between 0 and L. The parallel plates are heated with a uniform heat flux equal to $\dot{q}$, while the auxiliary plate heat flux can be 0 or $\dot{q}_p \neq 0$. An enlarged computational domain is chosen. It is made of the channel with auxiliary plate and of two reservoirs of height L_x and width L_y which are placed upstream and downstream of the channel. Due to thermofluidynamic and geometrical symmetries, the problem is solved in half the domain, as shown in Fig. 1(b).

The dimensionless Navier–Stokes equations in terms of stream function and vorticity, derived for a two-dimensional steady-state flow regime and with the Boussinesq approximation are

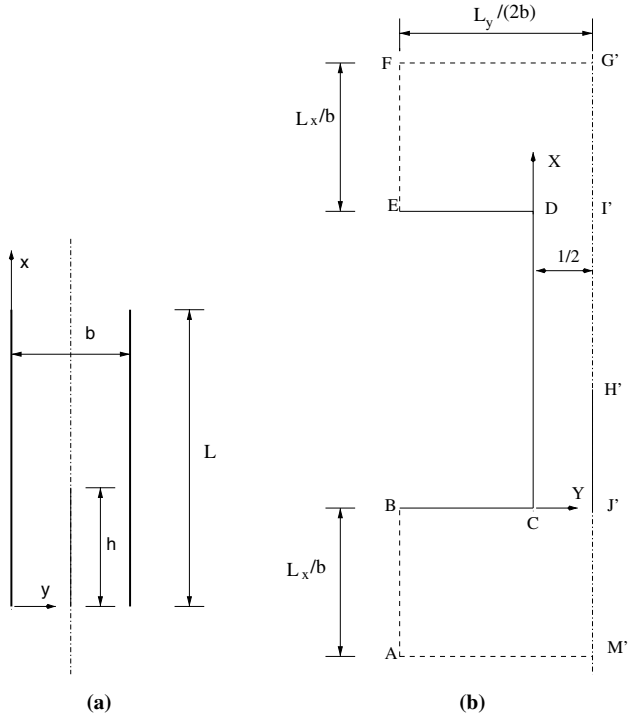

Fig. 1. Sketch of the vertical channel with auxiliary plate: (a) investigated configuration; (b) computational domain.

$$\frac{\partial(U\Omega)}{\partial X}+\frac{\partial(V\Omega)}{\partial Y}=\nabla^2\Omega-Gr\frac{\partial\theta}{\partial Y}, \tag{1}$$

$$\frac{\partial^2\Psi}{\partial X^2}+\frac{\partial^2\Psi}{\partial Y^2}=-\Omega, \tag{2}$$

where the dimensionless stream function and vorticity are

$$\frac{\partial\Psi}{\partial Y}=U,\quad \frac{\partial\Psi}{\partial X}=-V,\quad \Omega=\frac{\partial V}{\partial X}-\frac{\partial U}{\partial Y}. \tag{3}$$

The dimensionless energy equation, by neglecting the terms of dissipation and total derivative of pressure is (Gebhart et al., 1988)

$$\frac{\partial(U\theta)}{\partial X}+\frac{\partial(V\theta)}{\partial Y}=\frac{1}{Pr}\nabla^2\theta. \tag{4}$$

The dimensionless variables are defined as follow:

$$X=\frac{x}{b},\quad Y=\frac{y}{b},\quad U=\frac{ub}{\nu},\quad V=\frac{vb}{\nu},\quad P=\frac{(p-p_\infty)b^2}{\rho\nu^2},$$

$$\theta=\frac{(T-T_\infty)k}{\dot{q}b},\quad \Psi=\frac{\psi}{\nu},\quad \Omega=\frac{\omega b^2}{\nu},$$

$$Gr=\frac{g\beta\dot{q}b^4}{k\nu^2},\quad Pr=\frac{\nu}{a},\quad Ra=GrPr,\quad Ra^*=Ra\frac{b}{L},$$

$$x_q=\frac{\dot{q}_\mathrm{p}}{\dot{q}}. \tag{5}$$

Eqs. (1), (2) and (4) are solved by imposing the boundary conditions, with reference to Fig. 1(b), given in the following:

Ψ	Ω	θ	Zone
$\frac{\partial^2\Psi}{\partial Y^2}=0$	$\frac{\partial\Omega}{\partial Y}=0$	$\theta=0$	AB
$\frac{\partial^2\Psi}{\partial X^2}=0$	$\frac{\partial\Omega}{\partial X}=0$	$\theta=0$	AM′
$\Psi=\Psi_{\mathrm{w1}}$	$\frac{\partial\Psi}{\partial X}=0$	$\frac{\partial\theta}{\partial X}=0$	BC and DE
$\Psi=\Psi_{\mathrm{w1}}$	$\frac{\partial\Psi}{\partial Y}=0$	$\frac{\partial\theta}{\partial Y}=-1$	CD
$\Psi=\Psi_{\mathrm{w2}}$	$\frac{\partial\Psi}{\partial Y}=0$	$\frac{\partial\theta}{\partial Y}=x_q$	J′H′
$\frac{\partial^2\Psi}{\partial Y^2}=0$	$\frac{\partial\Omega}{\partial Y}=0$	$\frac{\partial\theta}{\partial Y}=0$	EF

The local convective heat transfer over the channel plate is described by the local Nusselt number, defined as

$$Nu(x)=\frac{h(x)b}{k}=\frac{1}{\theta_{\mathrm{w1}}(x)}. \tag{6}$$

Similarly, the local Nusselt number over the auxiliary plate, when heated, is

$$Nu_\mathrm{p}(x)=\frac{h_\mathrm{p}(x)b}{k}=\frac{x_q}{\theta_\mathrm{p}(x)}. \tag{7}$$

The average values can be written as

$$Nu=\frac{b}{L}\int_0^{L/b}Nu(X)\,\mathrm{d}X, \tag{8}$$

$$Nu_\mathrm{p}=\frac{b}{h}\int_0^{h/b}Nu_\mathrm{p}(X)\,\mathrm{d}X. \tag{9}$$

Moreover an average channel Nusselt number can be written as

$$Nu_\mathrm{c}=\left[\frac{1}{\theta_{\mathrm{w1av}}}+\left(\frac{h}{L}\right)\frac{x_q}{\theta_{\mathrm{pav}}}\right]\left(\frac{1}{1+(h/L)}\right), \tag{10}$$

where

$$\theta_{\mathrm{w1av}}=\frac{b}{L}\int_0^{L/b}\theta_{\mathrm{w1}}(X)\,\mathrm{d}X, \tag{11}$$

$$\theta_{\mathrm{pav}}=\frac{b}{h}\int_0^{h/b}\theta_\mathrm{p}(X)\,\mathrm{d}X. \tag{12}$$

3. Numerical procedure

The numerical solution to Eqs. (1)–(4) is carried out by employing the control volume method. Since in this case the induced mass flow rate is an unknown function of thermo-geometrical parameters such as L/b, h/L and the Rayleigh number, the stream function values on the channel plate, Ψ_{w1}, and on the centerline, Ψ_{w2}, are not known in advance. In fact, the $\Delta\Psi=\Psi_{\mathrm{w2}}-\Psi_{\mathrm{w1}}$ represents the induced volumetric flow rate in half the channel. The numerical solution is carried out by employing a false transient method and the steady-state solution to the problem is obtained as an asymptotic limit of the transient solutions. The problem is solved in the following steps:

1. assign a guessed $\Delta\Psi$ value;
2. solve Eqs. (1) and (4), using the ADI technique (Alternating Direction Implicit);
3. solve the stream function equation (Eq. (2)) by the SLOR method with an optimal value of the relaxation factor of about 1.7;
4. once the steady-state is attained, the guessed induced mass flow rate is checked. The selected value of the mass flow rate is verified by integrating the momentum equation along the centerline of the channel in the chosen computational domain. This condition must be verified

$$\int_{-L_x/b}^{(L_x+L)/b}\frac{\partial P}{\partial X}\,\mathrm{d}X=0. \tag{13}$$

If this equation is not satisfied within a prescribed accuracy (10^{-2}), return to step 1 and repeat the whole procedure until a converged solution is obtained.

The steady-state solution of the problem is attained as an asymptotic limit of the transient solutions. So a convergence criterion should be checked to test the attainment of the steady-state. The steady-state condition is considered to be reached when the variation of θ and Ω is less than 10^{-6}.

Preliminarily the dependence of the numerical solution on the mesh spacing was analyzed by monitoring the induced mass flow rate, $\Delta\Psi$, and the average Nusselt number, Nu. The induced mass flow rate values and the average Nusselt number values, at $Ra=10^4$ and with a number of nodes along X, n_X, equal to 51, for different numbers of nodes along Y are reported in Table 1.

It was observed that, by doubling the number of nodes along Y from 13 to 27, $\Delta\Psi$ and Nu showed a variation of about 1.5%. To obtain an accurate estimate of exact $\Delta\Psi$ and Nu values, used as reference values, a Richardson's extrapolation was used (Roache, 1998).

Table 1
$\Delta\Psi$ and Nu values at $Ra=10^4$ and $n_X=51$ for different numbers of nodes along Y

n_Y	$\Delta\Psi$	Nu
11	51.0	3.28
13	51.0	3.20
21	50.23	3.18
27	50.18	3.18

For $\Delta\Psi$ and Nu, it results:

$$\Delta\Psi_{\text{exact}} \cong \frac{4}{3}\Delta\Psi_{51\times27} - \frac{1}{3}\Delta\Psi_{51\times13} = 50, \tag{14}$$

$$Nu_{\text{exact}} \cong \frac{4}{3}Nu_{51\times27} - \frac{1}{3}Nu_{51\times13} = 3.173. \tag{15}$$

Therefore, the variations of the induced mass flow rate and average Nusselt number values, obtained when the number of nodes along Y is 27, respect to the reference values are 0.36% and 0.2%, respectively. A lesser dependence of the same variables was observed on the number of nodes along X. In the investigated cases a 27×51 uniform mesh is employed. Moreover, a reservoir height equal to two times the channel height and a horizontal width equal to 21 times the channel gap are sufficient to obtain a solution independent of the reservoir dimensions. This procedure was successfully tested by comparing its results with other numerical and experimental outcomes (Manca et al., 1994).

4. Results and discussion

In the following, results for Rayleigh number values between 10^3 and 10^6 are provided to point out the thermal and fluid dynamic characteristics of the channel. The results are obtained for air ($Pr = 0.71$) and channel aspect ratio L/b of 10. The auxiliary plate can be insulated, $x_q = 0.0$, or heated at the same uniform heat flux as the channel plate, $x_q = 1.0$.

4.1. Streamlines and isotherms

Streamlines and isotherms for a Ra value equal to 10^3 with an auxiliary plate with a height half of the channel plate, $h/L = 0.5$, are reported in Fig. 2.

The auxiliary plate is insulated ($x_q = 0.0$). At the channel exit, the stream function behaves like a jet in a free field. Fig. 2(a) shows that the fluid, heated by the channel plates and exiting the channel, gets into the upper reservoir and trails fluid from the surroundings. In this case, the dragging is due both to viscous and thermal effects; in fact, the fluid exiting the channel is hotter than the surroundings and releases heat to this. Moreover, a contraction of the streamlines upstream of the channel exit is observed. At the inlet the streamlines are aligned and the flow is driven into the channel with relatively modest accelerations. Inside the channel, the streamlines are parallel to each other and aligned with the channel plates. The isotherms form two plumes which break off the upper part of the walls at the channel outlet and a relatively consistent penetration of the thermal disturbance in the ambient is observed; this penetration is due to the relevance of the diffusive effects as compared to the convective ones when $Ra = 10^3$. At the channel inlet, modest thermal gradients along X are observed due to the diffusive effects again. The adiabatic auxiliary plate does not involve a substantial modification of the thermal field either in the channel or at the channel outlet.

The isotherms and the streamlines related to the same previous configuration are reported in Fig. 3 for $Ra = 10^6$ and $x_q = 0.0$. The streamlines appear packed close to the plates in the channel (Fig. 3(a)); this fact implies higher velocities and a smaller boundary layer thickness than the previous case ($Ra = 10^3$). Abrupt directional variations are noted close to the lower corner at the inlet section of the channel. At the channel outlet section there is a lesser drawing of fluid from the surroundings compared to the previous case because the thermal disturbance does not diffuse due to the relevance of the convective compared to the diffusive effects. The flow develops inside the channel downstream of the auxiliary plate. It should

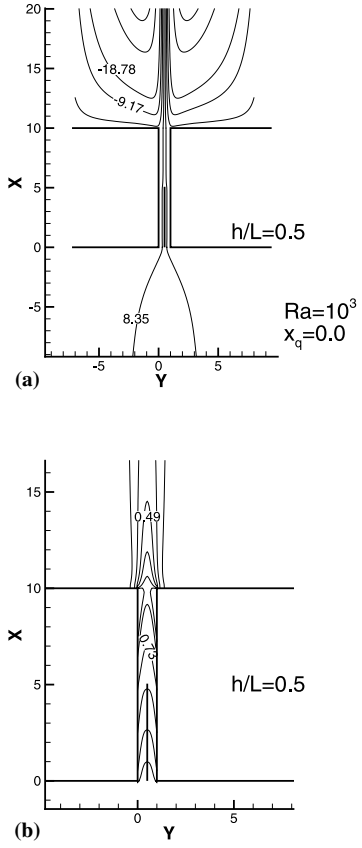

Fig. 2. Streamlines (a) and isotherms (b) at $Ra = 10^3$, $h/L = 0.5$ and $x_q = 0.0$.

be observed that the fluid thickens close to the hot walls of the channel downstream of the auxiliary plate. The isotherms, reported in Fig. 3(b), show that downstream of the outlet section the plume tends to move to the centerline and the thermal disturbance spreads into the surroundings to some extent.

The streamlines and the isotherms for Ra value of 10^3 and x_q equal to 1.0 with an auxiliary plate high half of the channel plate, $h/L = 0.5$, are reported in Fig. 4. The fluid in the channel sticks both to the auxiliary plate and to the channel plates for $X \leqslant 5.0$, whereas for greater X values the fluid departs from the plates, downstream of the auxiliary plate. This fact may be due to the presence of the plume placed downstream of the heated auxiliary plate on the centerline. In the upper reservoir, a contraction of the streamlines weaker than the corresponding case with $x_q = 0.0$ can be observed. Inside the channel the trend of the isotherms is clearly influenced by the heating of the central plate, as shown in Fig. 4(b). The temperature values of the auxiliary plate are very similar to those of the channel plates, at the same X value.

The streamlines and the isotherms, for a Ra value of 10^6 and x_q equal to 1.0 and at $h/L = 0.5$ are reported in Fig. 5. As the Ra value increases, the heated central plate influences markedly the draft from the lower reservoir, as shown in Fig. 5(a). Inside the channel, the streamlines are practically parallel to each other. As Fig. 5(b) shows, the thermal fields produce two plumes. These plumes lift off the two channel plates and practically do not interact with each other. At Rayleigh number value equal to 10^6, the thermal disturbance does not diffuse horizontally into the surroundings of the channel exit.

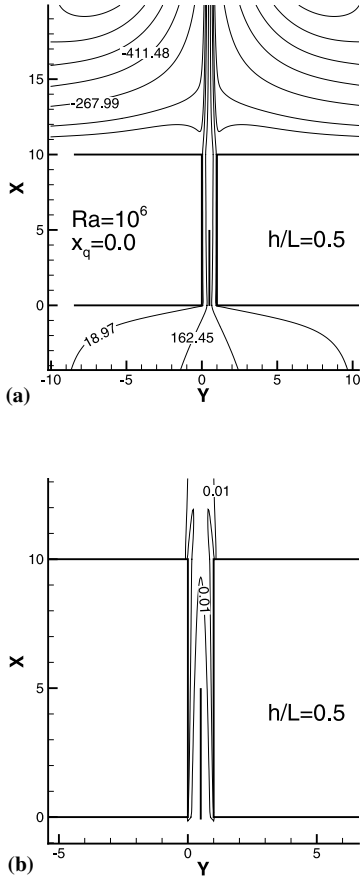

Fig. 3. Streamlines (a) and isotherms (b) at $Ra = 10^6$, $h/L = 0.5$ and $x_q = 0.0$.

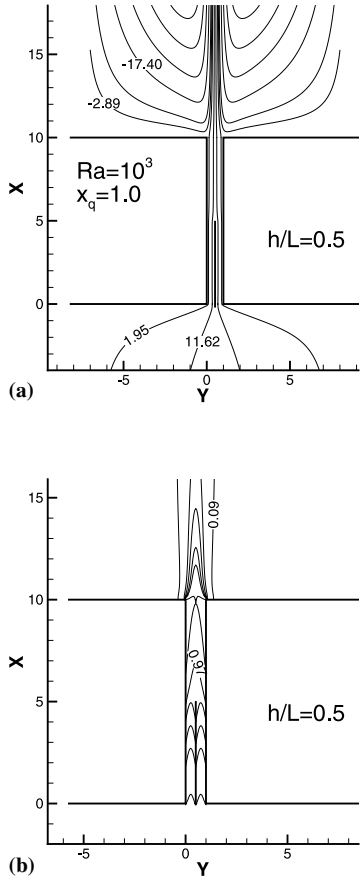

Fig. 4. Streamlines (a) and isotherms (b) $h/L = 0.5$ at $Ra = 10^3$, $h/L = 0.5$ and $x_q = 1.0$.

4.2. Velocity and temperature profiles inside the channel

Velocity and temperature profiles as functions of Y at different sections, for $Ra = 10^3$ and $Ra = 10^6$, for $x_q = 0.0$ and $x_q = 1.0$ are reported in Figs. 6 and 7. In these figures the ratio of the auxiliary plate height to the channel height, h/L, is equal to 0.0 and 0.5 and the profiles are reported to point out the thermal and fluid dynamic development inside the channel. The maximum velocity values in the channel and the wall temperatures of the profiles are given in Tables 2 and 3.

Fig. 6 shows that, at $h/L = 0.0$ (Fig. 6(a)), the velocity profile is partly deformed at the inlet, showing an approximately parabolic trend with a uniform zone in the core region. Moreover, the flow can be viewed as fully developed starting from $X = 5$ since the two profiles at $X = 5$ and 10 are virtually the same. The temperature profiles at the inlet ($X = 0$) present very low values in the core region compared to those adjacent to the wall. At the exit ($X = 10$), the temperature close to the wall increases less than that adjacent to the core region, due to the outer ambient cold air drawn by the plume jet toward the hot upper channel corner. The placement of the auxiliary plate modifies the velocity profile at the inlet section, producing a parabola at the sections where $X \leqslant 5$. At the inlet ($X = 0$), the velocity profiles are well developed for $h/L = 0.5$ (Figs. 6(b) and (c)). At the exit section ($X = 10$), when $h/L = 0.5$, the velocity profile is quite similar to that for the configuration without the auxiliary plate (Fig. 6(a)). At the channel inlet ($X = 0$), the temperature profiles are very similar to those corresponding to the case without auxiliary plate ("base case"). The auxiliary plate produces a uniform temperature profile; in fact, the central plate increases the diffusive effects because the Rayleigh number value is relatively low (10^3).

Fig. 7 shows that, for the base case (Fig. 7(a)), at the inlet section the velocity profile is flatter than when $Ra = 10^3$ and the flow increases. In fact, the profile at the exit section ($X = 10$) shows both an absolute maximum at about $Y = 0.12$ and a relative minimum at $Y = 0.5$. The temperature profiles show lower values than in the previous case ($Ra = 10^3$). Moreover, the fluid is practically undisturbed in the core zone of the channel, when $0.3 \leqslant Y \leqslant 0.5$, both at $X = 5$ and $X = 10$; this is due to the lower contribution of the diffusive effects because of high Rayleigh number value (10^6). The placement of the adiabatic auxiliary plate (Fig. 7(b)) does not modify the thermal behavior of the fluid compared to the base case while the velocity profiles are modified because of the no-slip condition on the auxiliary plate. At $h/L = 0.5$ and $x_q = 1.0$, the velocity profile asymmetry practically disappears at $X = 5$ (the heated auxiliary plate end) while the profile asymmetry is more pronounced at the inlet section (Fig. 7(c)): this is due to the heated auxiliary plate which realizes a better draft of the air while the flow close to the channel walls is not parallel to the walls for the corner presence. At the exit section the velocity values are practically uniform. A temperature profile asymmetry can be observed in Fig. 7(c), in the region where there is the auxiliary plate, for $h/L = 0.5$. Moreover, it is evident that the zone near $Y \cong 0.3$ is colder than the core region: this is due to the greater thermal boundary layer thickness of the channel plate than that adjacent to the auxiliary plate. In fact, close to the auxiliary plate, the flow is parallel while close to the channel walls the corner C at the channel inlet (see Fig. 1) can

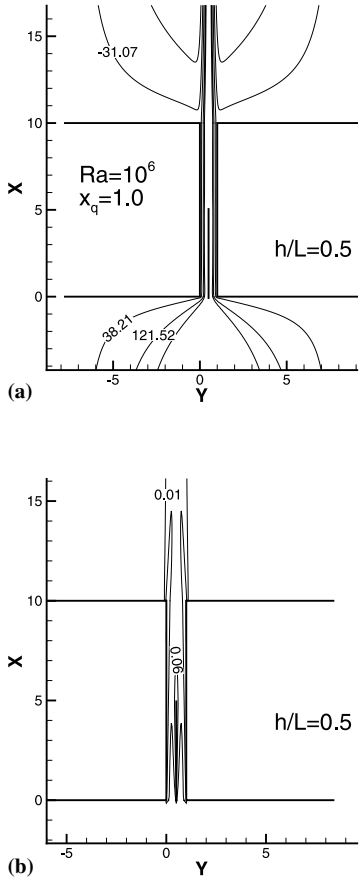

Fig. 5. Streamlines (a) and isotherms (b) at $Ra = 10^6$, $h/L = 0.5$ and $x_q = 1.0$.

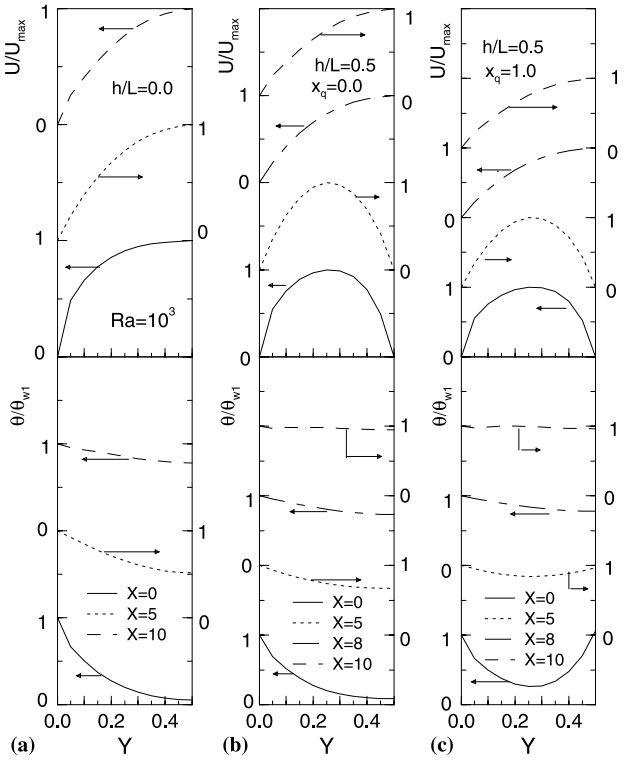

Fig. 6. $U/U_{\max}$ and θ/θ_{w1} profiles vs Y at different axial coordinates at $Ra = 10^3$: (a) $h/L = 0.0$; (b) $h/L = 0.5$ and $x_q = 0.0$; (c) $h/L = 0.5$ and $x_q = 1.0$.

produce a small flow recirculation downstream of the inlet section. At the channel exit the minimum temperature value is located at $Y = 0.5$.

4.3. Pressure profiles

The pressure profiles along the channel centerline are reported in Fig. 8. The Rayleigh number varies from 10^3 to 10^6 and the ratio of the auxiliary plate height to the channel height, h/L, is equal to 0.0, 0.5 and 1.0.

The pressure profiles for the base case ($h/L = 0.0$) show that the pressure drop at the channel inlet is greater, the higher the Ra value is, whereas the zone inside the channel with the minimum pressure is greater, the lower the Ra value is. This is due to the diffusion of the momentum. The pressure profiles along the centerline, for $h/L = 0.5$, for unheated ($x_q = 0.0$) and heated ($x_q = 1.0$) auxiliary plate show that the pressure decreases close to the inlet section, but there is a small, but sharp increase at $X = 0$, where there is an auxiliary plate. This is clearly evident only at $Ra = 10^3$ and $Ra = 10^4$ (Figs. 8(a) and (b)). Moreover, it is necessary to highlight a pressure reduction at the end of the auxiliary plate due to the increment of the velocity downstream to the central plate. When the auxiliary plate is heated ($x_q = 1.0$), the pressure reduction is due also to the thermal plume produced by the central plate. These effects are more relevant at the higher Ra values, thus a greater depression can always be observed when the auxiliary plate is heated ($x_q = 1.0$). At $Ra = 10^6$, the minimum pressure value is close to the inlet section for $x_q = 1.0$ (Fig. 8(d)) due to the "vena contracta" phenomena. When the auxiliary plate height

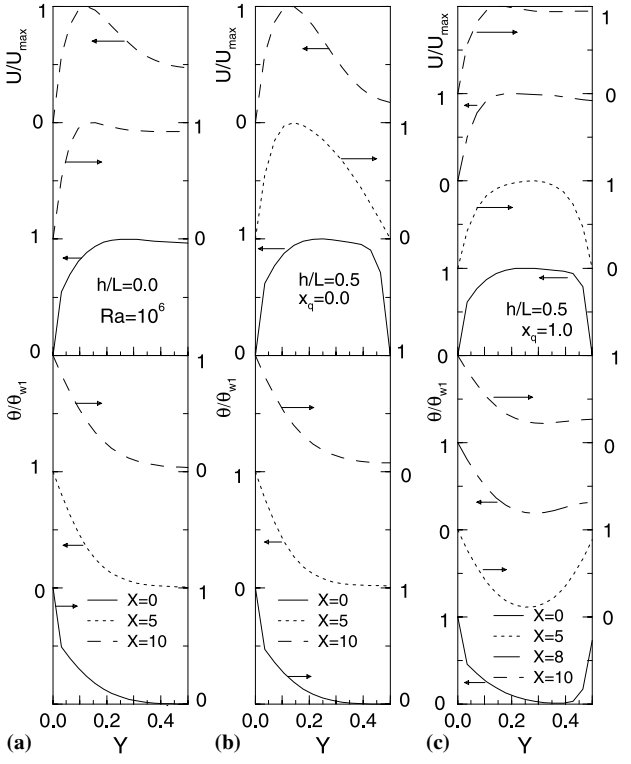

Fig. 7. $U/U_{\max}$ and θ/θ_{w1} profiles vs Y at different axial coordinates at $Ra = 10^6$: (a) $h/L = 0.0$; (b) $h/L = 0.5$ and $x_q = 0.0$; (c) $h/L = 0.5$ and $x_q = 1.0$.

Table 2
Maximum velocity values in the channel, U_{max}

	$Ra = 10^3$		$Ra = 10^6$	
$h/L = 0.0$				
$X = 0$	45.25		620.34	
$X = 5$	54.46		625.93	
$X = 10$	53.97		799.31	
	$Ra = 10^3$		$Ra = 10^6$	
	$x_q = 0.0$	$x_q = 1.0$	$x_q = 0.0$	$x_q = 1.0$
$h/L = 0.5$				
$X = 0$	33.07	42.19	535.16	790.27
$X = 5$	36.63	47.29	709.30	884.79
$X = 8$	36.32	47.53		777.07
$X = 10$	37.34	48.39	779.40	775.12
$h/L = 1.0$				
$X = 0$	27.13	37.39	503.53	768.16
$X = 5$	30.34	42.39	685.55	856.42
$X = 10$	29.25	41.23	773.88	807.53

Table 3
Maximum wall temperature values, θ_{w1}

	$Ra = 10^3$		$Ra = 10^6$	
$h/L = 0.0$				
$X = 0$	0.12		0.043	
$X = 5$	0.63		0.15	
$X = 10$	0.88		0.18	
	$Ra = 10^3$		$Ra = 10^6$	
	$x_q = 0.0$	$x_q = 1.0$	$x_q = 0.0$	$x_q = 1.0$
$h/L = 0.5$				
$X = 0$	0.13	0.12	0.048	0.046
$X = 5$	0.76	1.00	0.15	0.15
$X = 8$	1.14	1.36		0.17
$X = 10$	1.07	1.25	0.18	0.18
$h/L = 1.0$				
$X = 0$	0.14	0.13	0.049	0.046
$X = 5$	0.88	1.12	0.15	0.15
$X = 10$	1.24	1.67	0.18	0.18

is equal to the channel plate height ($h/L = 1.0$), the pressure behaves in a similar manner as before ($h/L = 0.5$) at the inlet section. Inside the channel, the pressure recover is similar to that of the base case. For $x_q = 1.0$ and at the lowest Ra values (10^3, 10^4) (Figs. 8(a) and (b)), the pressure attains lower minimum values as compared with to the case without the auxiliary plate due to the increase of the wall stress. This is caused by the presence of the auxiliary plate. The pressure reduction is more marked the higher the Ra value is.

The values of the induced mass flow rate ($\Delta\Psi$) are reported in Table 4. These values confirm the observations regarding the pressure profiles.

4.4. Heat transfer correlations

In this section correlations between average channel Nusselt number, Nu, Ra^* number and geometrical parameter, h/L, are proposed, for two x_q values:

$$Nu_c = 8.96 \cdot 10^{-2} \left(\frac{h}{L}\right)^{-0.029} (Ra^*)^{0.575} \quad \text{for } x_q = 0.0, \tag{16}$$

$$Nu_c = 4.42 \cdot 10^{-2} \left(\frac{h}{L}\right)^{0.0029} (Ra^*)^{0.894} \quad \text{for } x_q = 1.0. \tag{17}$$

The correlations are in the ranges: $10^2 \leqslant Ra^* \leqslant 10^5$ and $0.0 \leqslant h/L \leqslant 1.0$. In these correlations the dependence on h/L parameter is weak. In Eq. (16) the exponent is negative therefore the average channel Nusselt number decreases the higher one h/L value, whereas in Eq. (17) there is an opposite behavior. Furthermore, for $x_q = 1.0$, the channel Nusselt number changes approximately linearly with the channel Rayleigh number.

5. Conclusions

A numerical analysis of air natural convection in a symmetrically heated vertical heated channel with an auxiliary plate along the axial centerline of the channel to obtain the thermal and fluid dynamic characteristics of the system is presented. The analysis is carried out solving the fully elliptic Navier–Stokes and energy equations in terms of stream func-

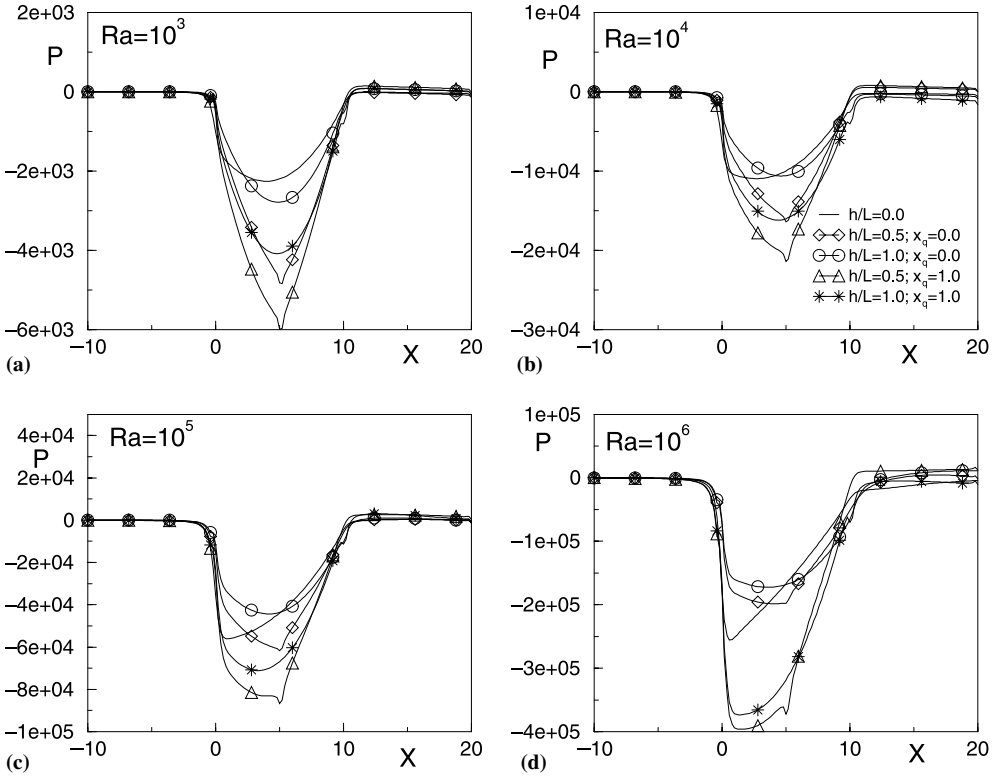

Fig. 8. Pressure profiles along the centerline at different h/L and x_q values and at different Ra values: (a) $Ra = 10^3$; (b) $Ra = 10^4$; (c) $Ra = 10^5$; (d) $Ra = 10^6$.

Table 4
Induced mass flow rate, $\Delta\Psi$, at different Ra, h/L and x_q values

	$Ra = 10^3$	$Ra = 10^4$	$Ra = 10^5$	$Ra = 10^6$
$x_q = 1.0$				
$h/L = 0.0$	18.75	51.00	127.06	280.00
$h/L = 0.5$	16.46	48.02	135.00	350.00
$h/L = 1.0$	14.50	44.16	126.34	340.00
$x_q = 0.0$				
$h/L = 0.5$	12.73	37.11	102.67	234.19
$h/L = 1.0$	10.36	31.75	90.30	220.0

tion – vorticity approach by the control volume method on a finite I-shaped computational domain.

The presence of the auxiliary plate modifies the fluid dynamic behavior of the channel. This is underlined by the streamlines and the temperature fields, the velocity and the temperature profiles inside the channel and by the pressure profiles along the centerline of the analyzed system. In particular, the presence of the adiabatic auxiliary plate produces a reduction of the drawing of the channel and modifies significantly the velocity profiles: this is due to increased loss of pressure along the solid walls. The placement of the adiabatic auxiliary plate does not modify qualitatively the thermal behavior of the fluid in the channel.

When the auxiliary plate is heated, a thermal plume is produced: this plume increases the drawing inside the channel. For the lowest Ra value (10^3), there is not induced mass flow rate increase because the viscous effect increase is stronger than that of the driving force. For the highest Ra value (10^6), however, the boundary layer thickness becomes lower and the driving force increase can prevail.

Correlations between channel Rayleigh number, dimensionless geometric parameter and average channel Nusselt number are proposed for $10^2 \leqslant Ra^* \leqslant 10^5$ and $0.0 \leqslant h/L \leqslant 1.0$. The dependence on h/L is weak and for $x_q = 1.0$ the exponent of the channel Rayleigh number in the correlation is close to unity (0.894).

Acknowledgements

This research was supported by the MURST with 1999 grant research program ''Enhancement Techniques in Thermofluids''.

References

Aihara, T., Ohara, T., Sasago, A., Ukaku, M., Gori, F., 1996. Augmentation of free-convection heat transfer between vertical

parallel plates by inserting an auxiliary plate. In: Second European Thermal Sciences, Rome, Italy, pp. 731–738.

Andreozzi, A., Manca, O., Morrone, B., 1999. Numerical analysis of natural convection in symmetrically heated vertical channels with an auxiliary parallel plate. In: NHTC-HTD/117, Albuquerque, NM, USA. ASME.

Bar-Cohen, A., Kraus, A.D., 1988. Advances in Thermal Modeling of Electronic Components and Systems, Vol. 1. Hemisphere, New York.

Campo, A., Manca, O., Morrone, B., 1997. Inflow and outflow effects on natural convection in partially heated vertical parallel plate channels. ASME-HTD 351, 325–335.

Campo, A., Manca, O., Morrone, B., 1999. Analysis of partially heated vertical parallel plates in natural convective cooling. Numer. Heat Transfer A 36, 129–151.

Cheng, C.H., Huang, W.H., Kou, H.S., 1988. Laminar free convection of the mixing flows in vertical channels. Numer. Heat Transfer A 14, 447–463.

Floryan, J.M., Novak, M., 1994. Free convection heat transfer in multiple vertical channels. Int. J. Heat Fluid Flow 16, 244–253.

Gebhart, B., Jaluria, Y., Mahajan, R., Sammakia, B., 1988. Buoyancy-Induced Flows and Transport. Hemisphere, Washington, DC.

Kim, S.J., Lee, S.W., 1996. Air Cooling Technology for Electronic Equipment. CRC Press, Boca Raton, FL.

Ledezma, G.A., Bejan, A., 1997. Optimal geometric arrangement of staggered vertical plates in natural convection. ASME J. Heat Transfer 119, 700–708.

Lee, K.T., 1994. Natural convection in vertical parallel plates with an unheated entry or unheated exit. Numer. Heat Transfer A 25, 477–493.

Manca, O., Morrone, B., Naso, V., 1994. A numerical study of natural convection between symmetrically heated vertical parallel plates. In: Atti del XII Congresso Nazionale sulla Trasmissione del Calore, L'Aquila, Italy. UIT, pp. 379–390.

Morrone, B., Campo, A., Manca, O., 1997. Optimum plate separation in a vertical parallel-plate channel for natural convection flows: incorporation of large spaces at the channel extremes. Int. J. Heat Mass Transfer 40, 993–1000.

Naylor, D., Tarasuk, J.D., 1993. Natural convective heat transfer in a divided vertical channel: Part 1. Numerical study. ASME J. Heat Transfer 115, 377–387.

Oosthuizen, P.H., 1984. A numerical study of laminar free convective flow through a vertical open partially heated plane duct. ASME HTD – Fundamentals of Natural Convection – Electronic Equipment Cooling 32, 41–48.

Peterson, G.P., Ortega, A., 1990. Thermal control of electronic equipments and devices. Adv. Heat Transfer 20, 181–314.

Raithby, G.D., Hollands, K.G.T., 1998. Handbook of Heat Transfer, third ed. McGraw-Hill, New York (Chapter 4).

Roache, J.P., 1998. Verification and Validation in Computational Science and Engineering. Hermosa, Albuquerque, NM.

Roberts, D.A., Floryan, J.M., 1998. Heat transfer enhancement in the entrance zone of a vertical channel. ASME J. Heat Transfer 120, 290–291.

Sparrow, E.M., Tao, W.Q., 1982. Buoyancy-driven fluid flow and heat transfer in a pair of interacting vertical parallel channels. Numer. Heat Transfer 5, 39–58.

Straatman, A.G., Tarasuk, J.D., Floryan, J.M., 1993. Heat transfer enhancement from a vertical, isothermal channel generated by the chimney effect. ASME J. Heat Transfer 115, 395–407.